

Combustion analysis of HCCI engine at different operating conditions

Y. Chandrasekharyadav*, Dr. D.V Sreekanth and Dr. Saurav Das

* Department of Mechanical Engineering, St. Martin's Engineering College, Telangana, 500100, India

* Correspondent Author: chandrasekharme@smec.ac.in

Submitted : 21/04/2020

Revised : 09/08/2020

Accepted : 10/10/2020

ABSTRACT

Automobile pollution is causing a huge trouble worldwide, and there is an urgent need to reduce it. Researches are being carried out for ways of reducing automobile pollution. The most common tool for converting liquid and gas fuel into useful mechanical work is the internal combustion (IC) engine. The explanation for its well-accepted efficiency, economics, longevity, controllability, and other competitive alternatives can be explained by its general appearance. NO_x and soot formation are due to the heterogeneous nonpremixed combustion of high local temperatures and the local oxygen shortage in the traditional direct injection diesel powered engine. The adjustment to the combustion cycle to boost engine output is an alternative to rising engine efficiency and reducing engine emissions. A simulation software with CFD code was implemented in this context, that is, the cold flow of the working conditions for HCCI engine control by creating a comprehensive model. Furthermore, the use of the in-cylinder model potential for cold flow simulation in the SI engine has been demonstrated. All strokes are replicated, pulling, compressing, expansion, and exhaust. The Discrete Phase System is used for injecting, evaporating, and boiling water, where the simulation depicts the working conditions of the engine for unravelling the flow physics taking place.

Keywords: HCCI Engine; CFD; IC engine; Alternative fuel.

1. INTRODUCTION

NO_x and soot formation are due to the heterogeneous nonpremixed combustion of high local temperatures and the local oxygen shortage in the traditional direct injection diesel powered engine (A. C. Alkidas. 2007). A suitable combustion control is implemented to prevent conditions in which particulates or NO_x are produced using alternative combustion methods. The adjustment to the combustion cycle to boost engine output is an alternative to rising engine efficiency and reducing engine emissions. An extremely effective way of doing so is combustion of a homogenous air/fuel mixture in the cylinder of a diesel engine. It provides a very powerful combustion system that can be used with different fuels (H. Machrafi et al. 2008). In certain ways, the Homogeneous Charge Compress Ignition (HCCI) combustion system blends the advantages of SI motor combustion with the homogeneous mixture of diesel engines (C.S. Daw et al. 2007). The CI engine fuel consumption and the SI engine emissions rate are achieved with HCCI (J.J. Hernandez et al. 2008). Several studies in recent years have shown that the formation of each pollutant can be

prevented by comprehensive load homogenization before combustion and a significant reduction in combustion gas temperature. Homogenous load compressed encounter is one of the methods.

The study can be divided into the following:

1. Generate a simulation program with CFD code: the cold flow of operating conditions for controlling the combustion timing of HCCI engine by building a detailed model.
2. The intake stroke and exhaust with a moving piston and valves will be modeled in the Computational Fluid Dynamics (CFD) package Fluent. The main problem with in-cylinder simulations is that the mesh, where the geometry is build out of, is moving and deforming. This requires a special treatment in the simulation setup. Since the speeds are high within the engine, the flow is turbulent.
3. For the turbulent flow characteristics, computational time is needed. Many process definitions in a turbulent flow are available; one of them is being implemented in this project.

2. CFD ANALYSIS FOR HCCI ENGINE

Air quality is obviously the role played by real-world mobile source emissions. Because the world is increasing, the need to build a cleaner engine has increased. It occurs in the automotive industry where there are intense competitive pressures to market new products in shorter times to respond rapidly to consumer needs. New engine developments such as direct fuel injection, turbo charging, gas exhaust recirculation, and treatment have been introduced more rapidly in this context. Without advances in CFD modeling, such recent developments would have been unlikely.

This is used to forecast fluid properties in the motor. This approach has very high overhead measurement but is invaluable as a tool to understand the airflow patterns in the engine more thoroughly. For model creation and implementation, various CFD codes, including KIVA, STAR CCD, FIRE, VECTIS, and FLUENT, were used. Mesh planning for 3D in-cylinder simulations of internal combustion engine phenomena is a bottleneck. Extreme fluid speeds are involved when modeling the flow of air in an internal combustion engine. Since these high speeds often suggest the presence of turbulence, the Reynolds number is significant. Turbulent flows are characterized by variable speed fields (X.C. Lu et al. 2005).

Turbulence consists of swirl-like structures, called eddies, of various dimensions. A chaotic but not necessarily random flux distinguishes turbulence. The calculated speed is not only local, but also a function of periods, expressed in two points in the flux. There is not a clear link when the flow is completely altered. Not all chaotic flows are necessarily turbulent; waves on the surface of the sea are a perfect example of a chaotic nonturbulent flux. In this part, different properties of turbulence will be discussed. First, the governing equations, which describe a viscous flow, will be treated. This set of equations includes the continuity, momentum, and energy equation. This section also includes the Reynolds-averaging method, which is used to reduce the computational cost of the solution of the governing equations. Secondly, the *Burgers equation* will be treated. With this relatively simple equation, the basics of turbulence can be solved analytically and give a better insight in this chaotic phenomenon. Kinetic energy is also an important quantity in turbulence. This will also be treated in this section. Vorticity is, with respect to the dynamics, the most important property. A compact definition of turbulence can be "*Chaotic vorticity.*" In governing equations, the dynamics of a flow can be represented. Three basic physical concepts are the basis for this classification, that is, (1) sea preservation; (2) impetus preservation (second law of Newton); (3) power management. An experimental study is performed for homogeneous charge compression ignition (HCCI) combustion focusing on late phasing conditions with high cyclic variability (CV) approaching misfire. It was observed that the available fuel does not necessarily burn during one cycle meaning that unburned fuel may carry over to the next cycle (Erik Hellström et al.

2012). In a study, four different valve mechanisms were used to extend HCCI operating range in a four stroke, single cylinder gasoline engine for 800 and 1900 rpm engine speeds. It was observed that the test engine was run on HCCI combustion mode at leaner air/fuel ratio as the inlet air temperature increased (Can Cinar et al. 2015). A work is carried out on the effects of residual gas fraction (RGF) on homogeneous charged compression ignition (HCCI) combustion, which was investigated experimentally. The experimental findings showed that in-cylinder pressure and heat release rate decreased using In5.5-Ex3.5 cam mechanism compared to In3.5-Ex3.5. More residual gases were trapped using In3.5-Ex3.5 cam mechanism (Can Cinar et al. 2016). Experimental results show that the volume fraction of n-butanol affects the knock tendency greatly, which obviously decreases as the n-butanol volume fraction increases. The knocking combustion in the HCCI combustion is characterized by the high heat release rate (HRR). Both elevating the engine speed and raising the intake temperature contribute to an obvious increase in HRR and the knock tendency (Gang Li et al. 2016). The results of comparison with the experimental data on density, isobaric heat capacity, enthalpy, and entropy of vaporization are presented. The comparison was performed over a temperature range of 300–630 K and pressures up to 60 MPa excluding the critical region. The average absolute deviations of the properties from optimized values are as follows: 0.17% for the liquid-phase density; 3.5% for the gas-phase density; 2.2% for the density in the supercritical region. The average absolute deviation of isobaric heat capacity for the liquid phase is 1.5–3.5%, for the gas phase, 2.5%, and in the supercritical region, 2.1% (Boris Grigoriev et al. 2018). Experiments were performed in a single-cylinder engine operated on methane/air. Spark ignition (SI) and homogeneous-charge compression-ignition (HCCI) were investigated. For HCCI, 5 mol% n-heptane was added to the fuel to reduce auto-ignition temperatures. With spark ignition at $\phi = 1.56$, the product gas contained up to 8.6 mol% CO and 7.7 mol% H₂ at 71.5% exergetic efficiency, while at $\phi = 0.72$ roughly, the same mechanical work was generated, but with only 42.5% exergetic efficiency (Sebastian Wiemann et al. 2018). By utilizing the promising alternative fuel of syngas, the syngas/diesel dual-fuel reactivity-controlled compression ignition (RCCI) is a potential combustion strategy for internal combustion engines. However, the optimal operating parameters for syngas/diesel RCCI engines under wide operating conditions have not been investigated. In this study, the operating parameters include fuel supply, syngas composition, and intake conditions of a syngas/diesel RCCI engine, which were optimized under wide load by integrating the KIVA-3V code and the nondominated sort genetic algorithm II (NSGA-II). The results indicated that nitrogen oxides (NO_x) emissions can be controlled in considerably low levels, and the efficient combustion of the premixed syngas in the squish region can be realized with high premix ratio and early pilot injection of diesel (Zhen Xu et al. 2018). A numerical model based on three-dimensional (3-D) computational fluid dynamics (CFD) was developed to capture knock in a Cooperative Fuel Research (CFR) engine. On the other hand, a novel methodology was also developed to analyze experimental data for the knocking case and identify the most representative cycle (CFR) engine (Pal, P., Kolodziej, C.P., Choi, S., Som, S. et al. 2018). A diesel engine was modified to operate as an electronically controlled HCCI-DI engine. TSDI strategy was applied by fixing the first injection timing in intake stroke and varying the second injection timing close to the compression top dead center (TDC). It can be understood from both experimental and CFD studies that combustion phase can be most effectively controlled by changing the second fuel injection timing for all fuel blends. Adding alcohol to gasoline helped decrease NO_x emissions while keeping the maximum cylinder gas pressure stable compared to pure gasoline (Ali Turkcan et al. 2018). A homogeneous compression ignition (HCCI) engine is taken for numerical investigation on the application of renewable fuels contained blends of methanol and DME with the base diesel fuel, which will be replaced with diesel in different percentages. The results indicate that the replacement of diesel with 20% of DME and 30% by methanol (D50M30DME20) at 1400 rpm generates a greater pressure and accumulated heat (AHR_{peak} ¼ 330.569 J), whereas D80M20/2000 rpm/EGR20 gives a defective combustive performance with poor engine efficiency (IMEP ¼ 7.21 bar) (Hadi Taghavifar et al. 2019). In this study, the effects of compression ratio on HCCI combustion, performance, and emissions were investigated parametrically. In addition to parametric investigation, and as a novel way of the paper engine BSFC maps were obtained for RON20 and RON40 fuels, each with a compression ratio of 9:1, 10:1, 11:1, and 12:1. The increase of octane amount of fuel led to the extension of combustion duration. On the contrary, combustion duration decreased along with the increase of compression ratio (Alper Calam et al. 2019).

2.1. Burgers Equation

Nonlinearity plays a fundamental role in turbulence. Because of this nonlinearity, the governing equations cannot be solved exactly. To gain a better insight into turbulence, the *Burgers equation* will be treated (J. Chang et al. 2006). This model is analytically manageable and contains the essential ingredients of a turbulent flow. It can be written as

$$\frac{\partial u}{\partial t} + u \frac{\partial u}{\partial x} = \nu \frac{\partial^2 u}{\partial x^2}$$

The second expression on the left-hand side of the *Burgers equation* is the nonlinear term and is called the convective term. It can be compared with the convection term in the *Navier-Stokes* equation. The expression on the right-hand side can be interpreted as friction. Both terms will be discussed separately in the following. First, only the friction term will be taken into account. The resulting equation is better known as the diffusion equation:

$$\frac{\partial u}{\partial t} = \nu \frac{\partial^2 u}{\partial x^2}$$

To come to a solution, a problem with the following begin and boundary conditions will be considered:

$$\begin{aligned} t = 0, & \quad u = I \delta(x) \\ x \rightarrow \pm\infty, & \quad u = 0 \forall t \end{aligned}$$

where $\delta(x)$ is the Dirac-delta-function and I is a constant that represents the magnitude of the velocity.

The solution of this problem reads as follows:

$$u = \frac{I}{2\sqrt{\pi\nu t}} e^{\frac{-x^2}{4\nu t}}$$

The solution is displayed in figure 2.1 for different values of t . For an increasing value of t , the gradient $\partial u = \partial x$ decreases. It can be concluded that friction is gradient-weakening. This is called stabilizing. Subsequently, the friction term will be omitted in equation 2.4. The resulting equation is called the nonlinear advection equation:

$$\frac{\partial u}{\partial t} + u \frac{\partial u}{\partial x} = 0$$

As can be seen, the transport velocity u is only a function of position x and time t . The general solution of this equation reads

$$u = f(x - ut)$$

where f is an arbitrary, differentiable equation. This equation shows that the velocity u in case of $t = 0$ travels unchanged in the $x; t$ -plane along the characteristic: $x - ut = \text{constant}$. The slope of this characteristic is $\partial x = \partial t = u$. This means that the slope is determined by the solution itself. This phenomenon is represented in figure 1. It can be seen from figure 2 that the gradient $\partial u = \partial x$ gets sharper as a function of the time. After a certain period, the solution

consists of more than one value. This is of course physically not possible. It can be concluded that the nonlinear term is gradient-sharpening, and this is called destabilizing.

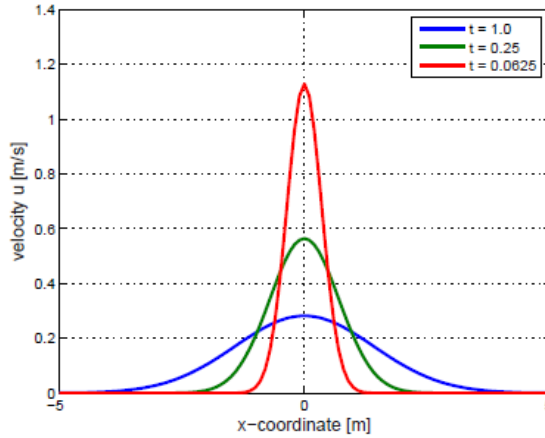


Figure 1. Solution of the diffusion equation at different periods in time. Initially, a triangular shape exists.

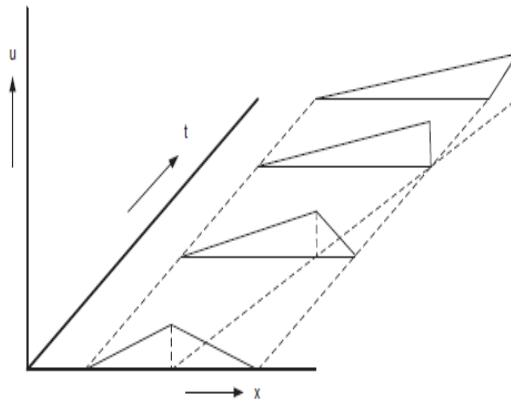


Figure 2. Solution of the nonlinear advection equation.

The behavior of equation can best be compared with the analogy of the shallow water waves. Waves at the beach break because the nonlinear effects make the waves steeper until their knock over and dissipate in the surf. In the previous part, two effects are treated, which influence the solution of the *Burgers equation*. These effects counteract. The first term is nonlinear, gradient-sharpening, and destabilizing. The second viscous term is gradient-weakening and stabilizing. The ratio between these two determines the solution of the Burgers equation. To characterize the ratio, this equation will be rewritten in dimensionless form. Therefore, a set of dimensionless variables will be defined.

$$\tilde{u} = \frac{u}{U}$$

$$\tilde{x} = \frac{x}{L}$$

$$\tilde{t} = t \frac{U}{L}$$

where \tilde{u} , \tilde{x} and \tilde{t} are the dimensionless velocity, position, and time. U and L are the velocity- and length scales. When substituted in equation, this results in the dimensionless Burgers equation

$$\frac{\partial \tilde{u}}{\partial \tilde{t}} + \tilde{u} \frac{\partial \tilde{u}}{\partial \tilde{x}} = \frac{1}{Re} \frac{\partial^2 \tilde{u}}{\partial \tilde{x}^2}$$

where $Re = UL/\nu$ is the Reynolds number. This number represents the ratio between the nonlinear advection term and the viscous term. When $Re < 1$, the viscous term dominates, and the flow is characterized as stable or laminar. When $Re \gtrsim 1$, the nonlinear advection term dominates, and the flow is unstable. In the last situation, the flow is characterized as turbulent.

To better understand what is happening at the different Reynolds numbers, the exact solutions of the Burgers equation will be treated. For a Reynolds number $Re \gg 1$, the term on the right-hand side of the above equation is negligible, and the solution is given by

$$u = \frac{u}{2} \left\{ -\tanh\left(\frac{ux}{4\nu}\right) + \frac{x}{L} \right\}$$

where $-L \leq x \leq L$ with

$$u = \frac{4U_0}{1 + \frac{2U_0 t}{L}}$$

In figure 18, the solution of the Burgers equation is plotted. With length scales in the order of L , the solution is dominated by the solution of the nonlinear equation 2.7. In this case, the exact solution can be approximated to

$$u = \frac{u}{2} \left\{ \frac{x}{L} + 1 \right\} \quad \text{for all } x < 0$$

$$u = \frac{u}{2} \left\{ \frac{x}{L} - 1 \right\} \quad \text{for all } x > 0$$

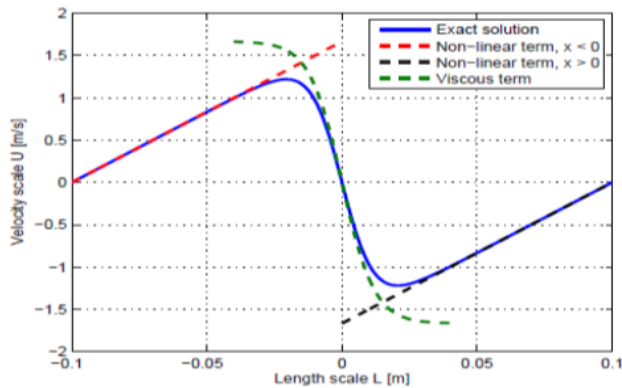


Figure 3. Exact solution of the Burgers equation for $Re \gg 1$.

2.2 Standard k - ε Model

The two-equation models are another class of turbulence models. The simplest is a regular k - ε model that Laundering and Spalding are providing (K. Yeom, J. Jang, Ch. Bae. 2007). Thanks to its overall applicability, solidity, and efficiency, it is commonly used in turbulence simulations. All kinetic energy and dissipation rate transportation equations are solved in a characteristic dimension, both at turbulent speed and longitude (L. Xingcai et al.2006) representing the turbulent viscosity of those measurements. The kinetic energy and dissipation rate equations (2.25) are given as follows:

$$\frac{\partial(\rho k)}{\partial t} + \frac{\partial(\rho \epsilon \overline{u_i})}{\partial x_i} = \frac{\partial[(\mu + \frac{\mu_t}{\sigma_k}) \frac{\partial k}{\partial x_j}]}{\partial x_j} + G_k - \rho \epsilon$$

$$\frac{\partial(\rho \epsilon)}{\partial t} + \frac{\partial(\rho \epsilon \overline{u_i})}{\partial x_i} = \frac{\partial[(\mu + \frac{\mu_t}{\sigma_\epsilon}) \frac{\partial \epsilon}{\partial x_j}]}{\partial x_j} + C_{1\epsilon} \frac{\epsilon}{k} G_k - C_{2\epsilon} \rho \frac{\epsilon^2}{k}$$

$$\mu_t = \rho C_\mu \frac{k^2}{\epsilon}$$

The turbulent viscosity is calculated using the following equation:

$$G_k = -\overline{\rho u'_i u'_j} \frac{\partial \overline{u_j}}{\partial x_i}$$

where C_μ is a constant. This is not direction-dependent and is not isotropic. The word G_k , at the end (X.C. Lu et al. 2005), is the generation of kinetic energy turbulence due to medium velocity gradients. This energy is supplied via the vortex stretching process to small scales by large scales (P. Yaping et al. 2007). This energy is dissipated into heat by small scales when hitting the Kolmogorov scales. G_k is calculated by means of the following equation (M.Canakci. 2008):

$$G_k = -\overline{\rho u'_i u'_j} \frac{\partial \overline{u_j}}{\partial x_i}$$

The equation for kinetic energy comes mathematically from this semiempirical model, while the equation for dissipation comes from physical reasoning. In addition, it is presumed that the low is fully turbulent and that the effects of molecular viscosities are negligible in the derivation of the typical k - ε model (M.F. Yao et al. 2009). This model is, therefore, true only for fully turbulent core streams. This is not normally a problem when the internal combustion engine is simulated.

2.3.RNG k - ε Model

The RNG k - ε turbulence model is derived from a framework called the "Restructure Group" (RNG) of the Navier-Stokes equations (M. Sjoberg, J. E. Dec. 2007). The study results in a model of constants different from those of the normal k2 model. In the transport equations for kinetic energy and dissipation, additional terms and functions will appear, which will be discussed below.

In the equations below, the transport equations of the RNG $k - \epsilon$ model are shown. They have a similar form as the standard $k - \epsilon$ model with a few differences (S. C. Kong and R. D. Reitz, Jul. 2002).

$$\frac{\partial(\rho k)}{\partial t} + \frac{\partial(\rho k \bar{u}_i)}{\partial x_i} = \frac{\partial(\sigma_k \mu_e f f \frac{\partial k}{\partial x_j})}{\partial x_j} + G_k - \rho \epsilon$$

$$\frac{\partial(\rho \epsilon)}{\partial t} + \frac{\partial(\rho \epsilon \bar{u}_i)}{\partial x_i} = \frac{\partial(\sigma_k \mu_e f f \frac{\partial k}{\partial x_j})}{\partial x_j} C_{1\epsilon} \frac{\epsilon}{k} G_k - C_{2\epsilon} \rho \frac{\epsilon^2}{k} - R\epsilon$$

The main difference with the standard $k - \epsilon$ model is an additional term $R\epsilon$ in the ϵ equation

$$R\epsilon = \frac{C_\mu \rho \eta^3 (1 - \frac{\eta}{\eta_0}) \epsilon^2}{1 + \beta \eta^3 k}$$

where $\eta = \frac{Sk}{\epsilon}$, $S = \sqrt{2S_{ij}S_{ij}}$, $S_{ij} = \frac{1}{2}(\frac{\partial u_i}{\partial x_j} + \frac{\partial u_j}{\partial x_i})$ the mean rate of the strain tensor and η_0 and β are constant.

$$-C_{2\epsilon}^* \rho \frac{\epsilon^2}{k} \text{ where } C_{2\epsilon}^* \equiv C_{2\epsilon} + \frac{C_\mu \rho \eta^3 (1 - \frac{\eta}{\eta_0})}{1 + \beta \eta^3}$$

R^2 is a positive factor in regions with relative low strain levels ($\eta < 0$), and $C_{2\epsilon}^* \epsilon$ is greater than $C_{2\epsilon} \epsilon$. The RNG model thus appears to produce results, which are largely comparable to the standard $k - \epsilon$ model for low to medium strained flows. At the other hand, the $R\epsilon$ term makes a negative contribution at high strain levels ($\eta > \eta_0$). The $C_{2\epsilon}^* \epsilon$ value is lower than the $C_{2\epsilon} \epsilon$ value. The smaller degradation of ϵ raises ϵ compared with the regular $k - \epsilon$ model, the k , and eventually effective viscosity. As a consequence, the RNG model produces less turbulent viscosity in strong stretching flows than the regular $k - \epsilon$.

$$d\left(\frac{\rho^2 k}{\sqrt{\epsilon \mu}}\right) = 1.72 \frac{\tilde{v}}{\sqrt{\tilde{v}^3 - 1 + C_v}} d\tilde{v}$$

Another difference with the standard $k - \epsilon$ model is the calculation of the turbulent viscosity. In case of the RNG model, the viscosity is calculated by the following equation:

$$\mu_t = \rho C_\mu \frac{k^2}{\epsilon}$$

2.4. Mesh Guidelines for the $k - \epsilon$ Models

The default option in FLUENT for $k - \epsilon$ turbulence models is the normal wall functions. Every wall-adjacent cell's centroid should be put under log-law, i.e., $30 < y^+ < 200$, for this type of wall feature and the nonequilibrium version. It is better to have a value similar to the lower bound. While FLUENT uses linear laminar law at 11:225, it is important to avoid using an overly fine mesh near the walls (Stenlås O. et al. 2004). This is because the wall

functions in the viscous sublayer are no longer true. We may use fine meshes, but then you must position the wall-adjacent cells in the layer of the buffer ($y^+ < 5$). The mesh instructions are specific when using the enhanced wall care. This wall feature is built to extend over the viscous sublayer the validity of near-wall modeling (X. C. Lu, W. Chen, Z. Huang. 2005). A mesh that completely addresses the accepted region of viscosity must therefore be constructed. This leads to an adjacent wall cell with a y^+ of the order 1. However, as long as it is well within the viscous sub layer, a higher value can occur (i.e., $y^+ < 4 \gg 5$). Another measure is that, in the viscosity-accepted area, there are at least 10 cells ($Key < 200$). The mean speed and turbulence amounts must be solved. The value of y^* should be about 11 to prevent an overly fine mesh.

Availability, stability, and efficiency are the advantages of the standard $k-\epsilon$ turbulence model. There would be no problem with the grid specifications ($30 < y^+ < 200$). The main downside is the semiempirical approach. Physical logic is used to formulate the equation for dissipation. It can be included or cannot be included in the following chapters. Lastly, the flow needs to be entirely turbulent, and the traditional $k-2$ model is therefore not ideal for wall-bound flows.

The RNG variable is a family member of the $k-\epsilon$ model. The grid needs of this model are similar. In the measurement of viscosity, the difference can be found. For small Reynolds, the viscosity of this model is measured in a different way, so that it can be used for low Reynolds and close-wall flows. Due to the high flow rate of the Reynolds engine simulation, this model probably is not more suitable than its regular counterpart.

The last member of the family $k-\epsilon$ is the pattern $k-\epsilon$. This model is perfect for flows that require a strong curvature, vortex, and rotation of streamline (S. C. Kong and R. D. Reitz. Jul. 2002). The mesh specifications are similar to the previous two versions and do not constitute an obstacle. In relation to the regular $k-\epsilon$, the turbulent viscosity of this model is anisotropic. This is probably the best choice for this model in the $k-\epsilon$ family.

3. MODELING AND ANALYSIS WITH FLUENT

The engine model in FLUENT is considered in the analysis, as a premixed turbulent combustion model. A high voltage is transmitted between two closely separated wires, producing a spark to start combustion at any given time and position into a combustion chamber. The spark event happens very rapidly in traditional engines compared with the main engine combustion. For a multidimensional engine simulation, the physical description of the basic event is detailed and complex and makes it difficult to accurately model the spark. Furthermore, the energy from the spark event is many orders of magnitude below the fuel release of chemical energy. Given the work into the physics of spark ignition and ignition devices, mixture inflammation at a point in the domain is more determined by the local composition than by the energy of the spark. Therefore, the spark event does not have to be modeled in great detail as the initiation of combustion over the lifetime of the user for circumstances, where FLUENT is used for combustion engine modeling, like internal combustion engines. As the spark ignition is essentially transient, only in the transient solver is the spark model available (K. Yeom, J. Jang, Ch. Bae. 2007). Furthermore, chemical reactions must be resolved in the spark model. The spark model is available for all combustion models but mainly for pre-premixed and partly pre-premixed combustion models. A one-dimensional study by Lipatnikov has contributed to the spark model used in FLUENT (H. Machraf, S. Cavadias, Ph. Guibert. 2008). The model is vulnerable to disruptions and can be unstable when used in multidimensional simulations. The instabilities are inherent to the model and can be mesh-dependent, particularly when the model reduces the discussion for the initial spark kernel growth to be simulated (K. Inagaki et al. 2006). Instability is likely to be compounded by numerical errors if the grid is not compatible with flame propagation. The effect of instability decreases as the spark nucleus increases and as the model allows turbulent mixes.

3.1 Analysis of 2D Cylinder Model

Perhaps one of the most complex engineering issues of computer fluid dynamics is the IC engine simulation. Port injection in multicylinder engines is used to effectively blend air/fuel and disperse fuel. In this analysis, the inlet and exit valves were considered as a two-dimensional engine. The engine is running at 2000 rpm. There are processes for intake, friction, expansion, and exhaust. Ports are modelled, and fuel droplets are evaporated. The fuel spray's contact with the inlet valve is based on FLUENT's wall film design (K. Yeom, J. Jang, Ch. Bae. 2007).

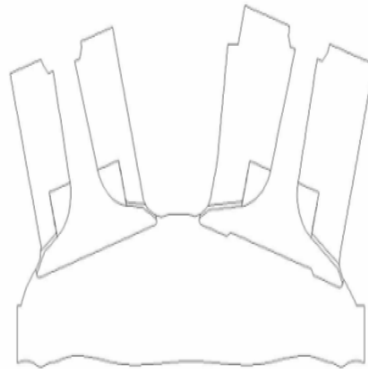


Figure 4. Dimensional model of cylinder with intake and exhaust valve.

The injection begins with 0.005 s and ends with 0.0111 s in this simulation. Whereas any other event is described by the crank angle such as piston motion, valve opening, and closing, FLUENT will repeat the event any 720 degrees, that is, crank time. Nevertheless, the crank angle of the injection event cannot be specified and, as a result, does not occur regularly. Regarding the limits for input and exit friction, the dynamic mesh movement of the piston and valves is facilitated for modeling in terms of the shaft angle of the crank, shaft speed, the piston stroke, and the length of the rod connecting. Furthermore, in terms of the angle of crank, it is progressed with the height of the crank angle. At present, the piston is in the top dead middle. The location of the TDC is established. The angles of degree of the crank are determined by the location Bottom Dead (BDC) of 180, 540, and 900.

With four-stroke motors, there is a value of 720 degrees, and for two-stroke motors, a value of 360 degrees is used. The regularity of the events and the valve lift profiles is controlled. By default, the zone is not taken into consideration when upgrading the mesh to the next level, where the attributes of the motion (moving or deforming), no face or cell zone, are allocated. In this case, however, a stationary zone explicit declaration is necessary.

Due to the assignment of solid body motions to the inner adjacent cell zone, the locations of all nodes belonging to these cell areas are changed even though the interiors connected with the nodes are part of the nonrunning boundary region (L. Xingcai et al. 2006).

When the node positions are modified, the nodes are removed by explicit declaration of a stationary field. By default, the zone is not taken into consideration when upgrading the mesh to the next level where the attributes of the motion (moving or deforming), no face or cell zone, are allocated. In this case, however, a stationary zone explicit declaration is necessary. Based on the assignment of a solid body movement in the internal adjacent cell zone (ex-ib and in-ib), the locations of all the nodes in these cell zones will be upgraded unlike the nodes in the inner zone.

4. RESULTS

Figure 5 displays a cylindrical mass plot in the motorcycle motor simulation. The loss rate from the model is proportional to the pressure difference in the interface between the cylinders and the crankcase. Figures 6–16 display a cylindrical pressure plot for the same motor simulation. In proportion to the overall mass loss from the cylinder, the mass loss from the grid is to lower the peak pressure. Figure 10 displays the static temperature distribution, which shows the nature of flow physics.

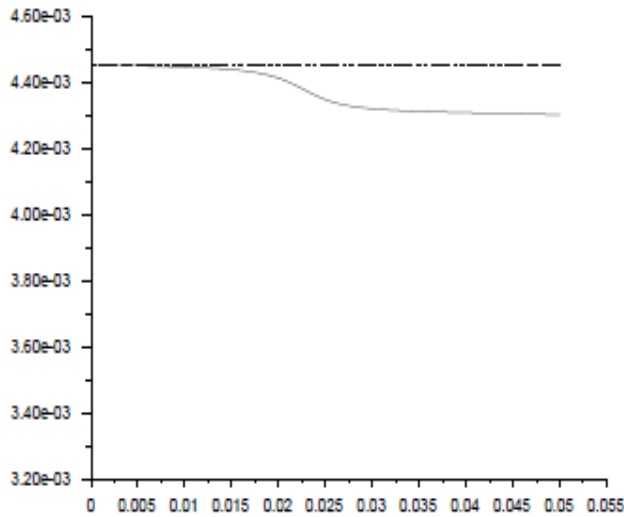
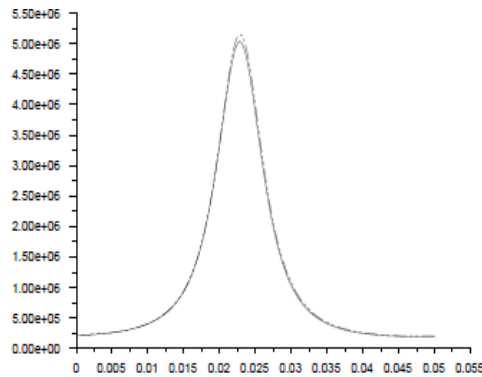


Figure 5. Cylinder Mass vs. Crank Angle.



Cylinder Pressure vs Time (Time=0.0000e+00)

Figure 6. Figure 6. Cylinder Pressure vs. Crank Angle.

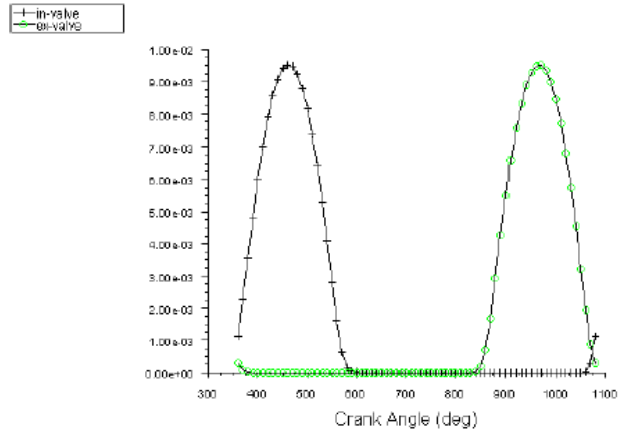


Figure 7. Piston Motion Profile.

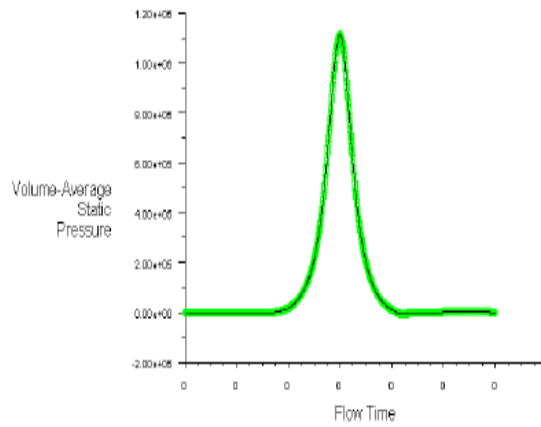


Figure 8. Convergence History of Static Pressure.

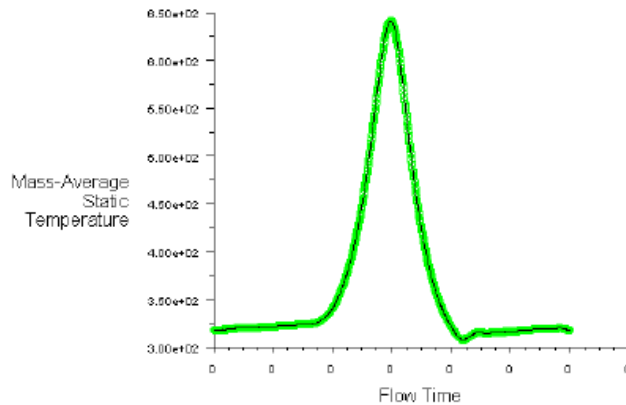


Figure 9. Convergence History of Static Temperature.

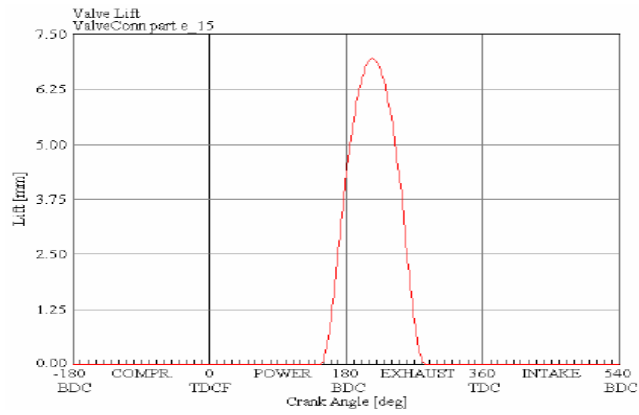


Figure 13. Exhaust valve lift.

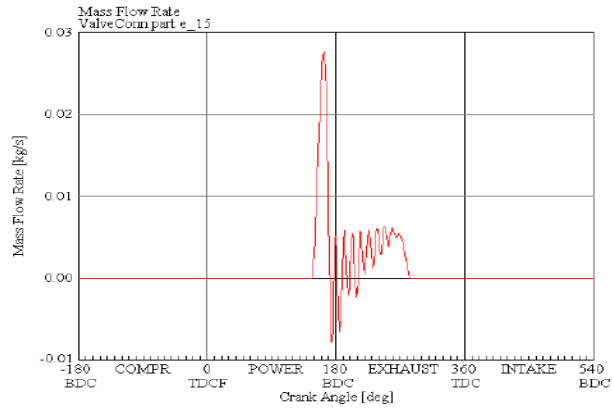


Figure 14. Mass flow rate in exhaust valve.

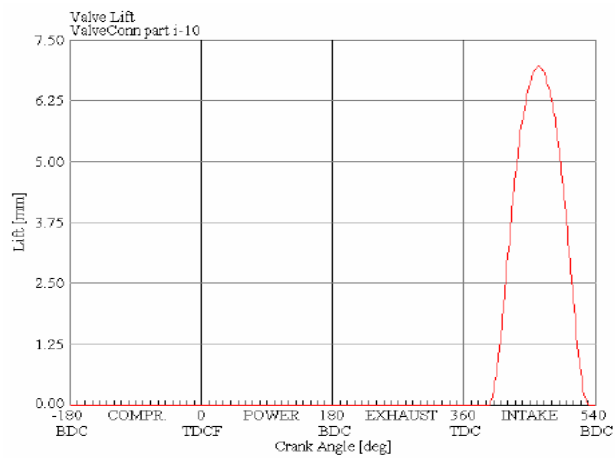


Figure 15. Intake valve lift.

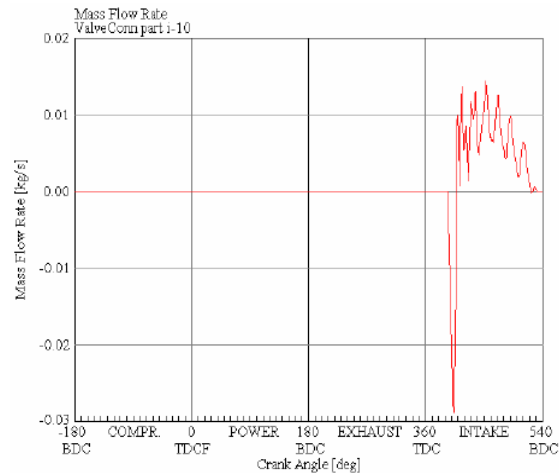


Figure 16. Mass flow rate in intake valve.

5 CONCLUSION AND FUTURE SCOPE

The cold flow simulation within the SI engine use of In-Cylinder model features has been illustrated. Simulation of all strokes, suction, compression, expansion, and exhaust is done. The Discrete Step Model simulates the injection of gasoline, evaporation, and boiling gout. The outcome of the simulation of intake and exhaust stroke in an engine cylinder shows that the simulation begins at the top dead center (TDC) and ends at 7200 of the crank revolution for a temporary period. Inert air scalars are used to control the intake and exhaust stream through exhaust packs in the motor cylinders. During the simulation, port limit pressures are maintained continuously in ambient conditions. The mesh architecture of a moveable mesh and the changing cell connectivity is controlled by the need to keep the component grid's dynamic mesh simple, so that it can be easily modified in the transitional cycle. In these issues, the formulation of mesh movement in two conceptual stages is split. The first issues changed communication identified by different events. The second step consists in determining the location of the grid vertex in function of the time, providing a set of dynamic grid handling commands that will be performed at each step. A mesh movement is possible, and grid manipulation is effectively carried out with dynamic mesh control. The Realizable $k - \mu$ model in case of the organized mesh is the most effective model. The virtual origin and the constant velocity decline are both predicted. Compared to its structured counterpart, the unstructured mesh version is less effective, but for this type of mesh, it is still one of the best models. To increase engine models output, the combustion model of different fuel for HCCI motor can still be validated as further extension, based on the validation of variable valve schedules for the HCCI motor.

REFERENCES

- Alper Calam, Hamit Solmaz, Yakup Icingur, Emre Yılmaz. 2019.** Investigation of Effect of Compression Ratio on Combustion and Exhaust Emissions in A HCCI Engine, S0360-5442(18)32389-2.
- A. C. Alkidas. 2007.** Combustion advancements in gasoline engines, International Journal of Energy Conversion and Management, 48: 2751- 2761.

- Ali Turkcan, Mustafa Deniz Altinkurt, Gokhan Coskun, Mustafa Canakci. 2018.** Numerical and experimental investigations of the effects of the second injection timing and alcohol-gasoline fuel blends on combustion and emissions of an HCCI-DI engine, *Fuel*: 219, 50-61.
- Boris Grigoriev, Igor Alexandrov, Anatoly Gerasimov. 2018.** Application of multiparameter fundamental equations of state to predict the thermodynamic properties and phase equilibria of technological oil fractions, *Fuel*: 215, 80-89.
- Can Cinar, Ahmet Uyumaz, Hamit Solmaz, Tolga Topgul. 2015.** Effects of valve lift on the combustion and emissions of a HCCI gasoline engine, *Energy Conversion and Management* : 94, 159–168.
- Can Çinar, Ahmet Uyumaz, Seyfi Polat, Emre Yılmaz, Özer Can, Hamit Solmaz. 2016.** Combustion and performance characteristics of a HCCI engine utilizing trapped residual gas via reduced valve lift, *Applied Thermal Engineering*, S1359-4311(16)30223-X, 1-26.
- C. S. Daw, R. M. Wagner, K. D. Edwards, J. B. Green. 2007.** Understanding the transition between conventional spark-ignited combustion and HCCI in a gasoline engine, *Proceedings of the Combustion Institute*, :31, 2887–2894.
- Erik Hellström, Anna Stefanopoulou, Jiri Vavra, Aristotelis Babajimopoulos, Dennis Assanis, Li Jiang and Hakan Yilmaz. 2012.** Understanding the dynamic evolution of cyclic variability at the operating limits of HCCI engines with negative valve overlap, *SAE International*, 01-1106.
- Gang Li, Chunhua Zhang, Jiawang Zhou. 2016.** Study on the knock tendency and cyclical variations of a HCCI engine fueled with n-butanol/n-heptane blends, *Energy Conversion and Management* xxx, xxx–xxx.
- H. Machrafi, S. Cavadias, Ph. Guibert. 2008.** An experimental and numerical investigation on the influence of external gas recirculation on the HCCI auto-ignition process in an engine: Thermal, diluting, and chemical effects, *International Journal of Combustion and Flame*.
- Hadi Taghavifar, Arash Nemati, Jens Honore Walther. 2019.** Combustion and exergy analysis of multi-component diesel-DME methanol blends in HCCI engine, *Energy*: 187, 115951.
- J. Chang, Z. Filipi, D. Assanis, T-W Kuo, P. Najt, R. Rask. 2005.** Characterizing the thermal sensitivity of a gasoline homogeneous charge compression ignition engine with measurements of instantaneous wall temperature and heat flux, *International Journal of IMechE*.
- J.J. Hernandez, J. Sanz-Argent, J. Benajes, S. Molina. 2008.** Selection of a diesel fuel surrogate for the prediction of auto-ignition under HCCI engine conditions, *International Journal of Fuel*: 87, 655–665.
- K. Inagaki, T. Fuyuto, K. Nishikawa, K. Nakakita, I. Sakata. 2006.** Combustion system with premixture-controlled compression ignition, *R&D Review of Toyota CRDL Vol.41 No.3*.
- K. Yeom, J. Jang, Ch. Bae. 2007.** Homogeneous charge compression ignition of LPG and gasoline using variable valve timing in an engine, *International Journal of Fuel*: 86, 494-503.
- L. Xingcai, H. Yuchun, Z. Linlin, H. Zhen. 2006.** Experimental study on the auto-ignition and combustion characteristics in the homogeneous charge compression ignition (HCCI) combustion operation with ethanol/n heptane blend fuels by port injection, *Fuel*: 85, 2622–2631.
- M. Canakci. 2008.** An experimental study for the effects of boost pressure on the performance and exhaust emissions of a DI-HCCI gasoline engine, *International Journal of Fuel*: 87, 1503-1514.
- M. Sjöberg, J. E. Dec. 2007.** Comparing late-cycle autoignition stability for single- and two-stage ignition fuels in HCCI engines, *Proceedings of the Combustion Institute*: 31, 2895–2902.
- M. F. Yao, Z. L. Zheng and H. F. Liu. Oct. 2009.** Progress and recent trends in homogeneous charge compression ignition (HCCI) engines, *Prog. Energy Combust Sci*: 35, pp. 398-437.

- P. Yaping, T. Manzhi, G. Liang, L. Fafa, L. Hua, G. Yingnan. 2007.** Study the ethanol SI/HCCI combustion mode Transition by using the fast thermal management system, *Chinese Science Bulletin*: **52**, (19) , 2731-2736.
- Pinaki Pal, Christopher P. Kolodziej, Seungmok Choi, Sibendu Som, Alberto Broatch, Josep Gomez-Soriano, Yunchao Wu, Tianfeng Lu, Yee Chee See. 2018.** Development of a Virtual CFR Engine Model for Knocking Combustion Analysis, SAE International, 01-0187.
- S. C. Kong and R. D. Reitz. Jul. 2002.** "Use of detailed chemical kinetics to study HCCI engine combustion with consideration of turbulent mixing effects," *J. Eng. Gas Turb. Power-Trans ASME*, vol. 124, pp. 702-707.
- Stenlås O., Christensen M., Egnell R., Johansson B., Mauss F. 2004.** Hydrogen as Homogeneous Charge Compression Ignition Engine Fuel. SAE Technical Paper Series 2004, (04SFL-229).
- Sebastian Wiemann, Robert Hegner, Burak Atakan, Christof Schulz, Sebastian A. Kaiser. 2018.** Combined production of power and syngas in an internal combustion engine – Experiments and simulations in SI and HCCI mode, *Fuel*: 215, 40-45.
- Zhen Xu, Ming Jia, Yaopeng Li, Yachao Chang, Guangfu Xu, Leilei Xu, Xingcai Lu. 2018.** Computational optimization of fuel supply, syngas composition, and intake conditions for a syngas/diesel RCCI engine, *Fuel*: 234, 120-134.
- X. C. Lu, W. Chen, Z. Huang. 2005.** A fundamental study on the control of the HCCI combustion and emissions by fuel design concept combined with controllable EGR. Part 2. Effect of operating conditions and EGR on HCCI combustion," *International Journal of Fuel*: 84, 1084-1092.
- X. C. Lu, W. Chen, Z. Huang. 2005.** A fundamental study on the control of the HCCI combustion and emissions by fuel design concept combined with controllable EGR. Part 1. The basic characteristics of HCCI combustion," *International Journal of Fuel*: 84, 1074-1083.